Force Analysis of an Open TBM Gripping-Thrusting-Regripping Mechanism

Tian Huang[a,b], Xiaolong Wang[a], Haitao Liu[a], Yuhu Yang [a,*]

[a]*Key Lab. of Mechanisms Theory and Equipment Design of the State Education Ministry, Tianjin University, Tianjin 300072, China*

[b]*School of Engineering, The University of Warwick, Coventry CV4 7AL, UK*

Abstract:

This paper presents an approach for the force analysis of an open TBM gripping-thrusting-regripping mechanism, which is a special parallel mechanism driven by hydraulic actuators and constrained by rocky surroundings. The static equilibrium equations of the cutterhead-mainbeam-saddle subassembly are formulated first by exploring the reaction forces in the cross pin situated between the saddle and the gripper cylinder. This is followed by formulating the static equilibrium equations of the inner closed loops formed by the above subassembly, the torque and gripper cylinders. Consequently, the linear map between the externally applied wrench imposed on the shield and the equivalent thrust forces of the cylinders is developed. The functionality of the force model developed is twofold, i.e. it can be used either to estimate the thrust forces of the cylinders required to resist against the tunneling loads, or to predict the tunneling loads using the measured thrust forces of these cylinders, thus providing important theoretical basis for the design and control of the mechanism.

Key words: *Open TBM Gripping-Thrusting-Regripping Mechanism, Force Analysis*

Nomenclature

$\boldsymbol{R}$	Rotation matrix of the $O'-uvw$ with respect to the $O-xyz$
$\boldsymbol{a}_{i2}$, $\boldsymbol{b}_{i2}$	Position vector of A_{i2} and B_{i2} evaluated in the $O-xyz$
$\boldsymbol{a}_{i1}$, $\boldsymbol{b}_{i1}$, $\boldsymbol{d}$	Position vectors of A_{i1}, B_{i1} and D evaluated in the $O-xyz$
$\boldsymbol{a}_{0i1}$, $\boldsymbol{b}_{0i1}$, $\boldsymbol{d}_0$	Position vector of A_{i1}, B_{i1} and D evaluated in the $O'-uvw$
$l_{a,i}$, $\boldsymbol{s}_{a,i}$	Length and unit vector of the *i*th propel cylinder
$l_{b,i}$, $\boldsymbol{s}_{b,i}$	Length and unit vector of the *i*th torque cylinder
$\$_{w,L}$	Tunneling wrench with respect to O'
$f_{a,i}$	Thrust force of the *i*th propel cylinder
$f_{b,i}$	Thrust force of the *i*th torque cylinder
$f_{d,x}$, $f_{d,z}$	Reaction forces of the cross pin at *D* along the *x* and *z* axes
f_u, f_v	Resultant reaction forces imposed by the surrounding rock along the *u* and *v* axes at O'
f_{drag}	Drag resistance of the ground support equipment
$\boldsymbol{c}_b$, $\boldsymbol{c}_s$	Position vectors of the centroids of the main beam and saddle evaluated in the $O-xyz$
R	Radius of the shield
m_p, m_b, m_s	Masses of the shield (including the cutterhead), the main beam and the saddle
μ_f	Static friction coefficient of the surrounding rock
$\boldsymbol{f}_C$	Reaction force of the prismatic joint connecting the main beam with the saddle
$\boldsymbol{f}_{h_1}$, $\boldsymbol{f}_{h2}$	Reaction forces at the spherical joints of the gripper shoes
f_e	Difference between the thrust forces in two chambers of the gripper cylinder
$\$_w$	Equivalent externally applied wrench imposed upon the shield
$\hat{\$}_{w,a}$	Equivalent unit wrench of the propel cylinders
$\hat{\$}_{w,bl}$, $\hat{\$}_{w,br}$	Equivalent unit wrench of the left and right torque cylinders
$\hat{\$}_{w,e}$	Equivalent unit wrench of the gripper cylinder
$\hat{\$}_{w,u}$, $\hat{\$}_{w,v}$	Equivalent unit wrench of constraints imposed upon the shield by the surrounding rock
$\boldsymbol{W}$	Force Jacobian
$\boldsymbol{W}_a$, $\boldsymbol{W}_c$	Force Jacobian of actuations and constraints

* Corresponding author. Tel./fax: +86 2227405280
E-mail addresses: yangyuhu@tju.edu.cn, (Yuhu. Yang)

$\$_{w,G}$ Wrench produced by gravity and drag resistance

1. Introduction

Over the last few decades, open tunnel boring machine (TBM) has been widely used in infrastructure constructions such as underground/rail transportation and water conservancy, etc. [1]. The gripping-thrusting-regripping mechanism (GTRM) [2] in open TBM plays an important role for implementing continuous, efficient and accurate tunneling. In practice, two issues maybe encountered in the design and control aspects. The first is to design the hydraulic system that enables to provide sufficient thrust forces required to resist against the tunneling loads. The second is to predict the tunneling loads imposed upon the cutterhead by measuring the thrust forces of hydraulic cylinders such that online compliant control can be implemented. Both issues constitute the forward and inverse force analysis problems of the mechanism.

The open TBM GTRM is a special parallel mechanism driven by multiple hydraulic cylinders and constrained by rocky surroundings. Although a couple of useful methods have been available for the force analysis of parallel mechanisms, the Newton-Euler method [3-7], the virtual work principle [8-13], and the screw theory method [14-17], for example, it is important to note, however, that the GTRM operates under the constraints of rocky surroundings. Because of this very special working condition, the translational movements normal to the cutterhead's axis are uncontrollable. Moreover, the GTRM contains the branched kinematic chains that form the inner loop closures [18] and the oil circuits of some hydraulic actuators are connected. All these features make the force analysis of the GTRM quite different from that of the conventional parallel mechanisms having certain degrees of freedom and simple limb structures. An exhausted literature review shows that little work was reported for the force analysis of such mechanism [19-21].

Drawing mainly on the practical needs for the design and control, this paper investigates a method for the force analysis of an open TBM GTRM with particular interest in establishing the relationship between the tunneling loads and the thrust forces of hydraulic cylinders. Two examples are given to illustrate how this model could be used to estimate the thrust forces required to resist against the tunneling loads, and to predict the tunneling loads provided that the thrust forces of these cylinders can be obtained online.

2 System Description

The CAD and explosive models of the GTRM under consideration are shown in Fig.1. The mechanism is composed of the cutterhead, shield, main beam, four torque cylinders, saddle, four propel cylinders, gripper cylinder, gripper shoes and rear supporting legs. For the convenience of force analysis, the cutterhead, mainbeam and shield are treated as one body by locking the gear transmissions between the cutterhead and mainbeam as well as by locking the hydraulic cylinders between the main beam and shield. Two propel cylinders on the left/right side are placed in parallel manner and each of them is connected with the main beam at one extremity and with a gripper shoe at the other by a spherical joint. Two torque cylinders on the left/right side are placed in parallel and each of them is connected with the saddle and the gripper cylinder by a spherical joint. In addition, the saddle is connected with the gripper cylinder by the cross pin (composed of a prismatic joint and a spherical joint). The gripper cylinder is connected with the gripper shoe by a spherical joint at each end. The schematic diagram of the GTRM is shown in Fig.2, and its topological structure is given in Fig.3. Here, S and P represent the spherical and prismatic joint, respectively, and the underlined P represents the actuated prismatic joint (i.e. hydraulic cylinder). It is easy to see that the torque cylinders, the saddle and the cross pin form the inner loops between the gripper cylinder and the prismatic joint situated on the saddle.

It should be pointed out that unlike the redundantly actuated parallel mechanisms [22] in which all actuators are assumed to be linearly independent, the hydraulic circuits of the propel cylinders, torque cylinders and gripper cylinder

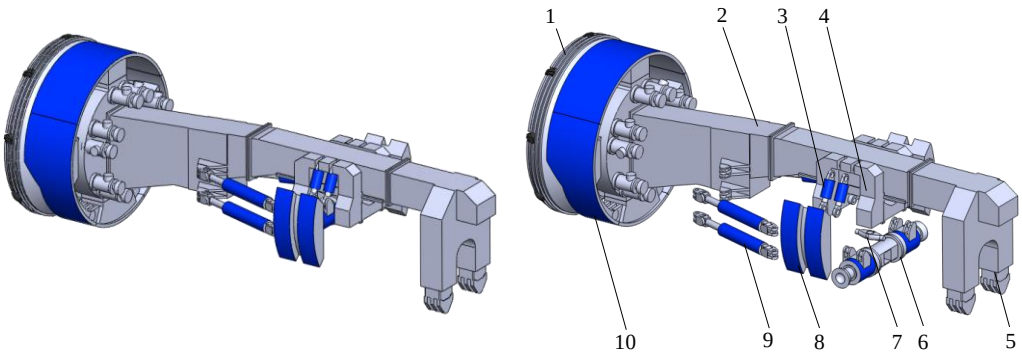

1.cutterhead, 2.mainbeam, 3.torque cylinder, 4.saddle 5.rear supporting leg, 6.gripper cylinder, 7.cross pin 8.gripper shoe, 9. propel cylinder, 10. shield

Fig.1. CAD model(left) and explosive model(right) of the GTRM

are intentionally designed as follows. The hydraulic circuits of all four propel cylinders are connected, leading to the same thrust forces in these cylinders. This treatment actually produces one independent actuation to resist against the tunneling load along the cutterhead axis and to balance the frictional moment arising from gravity of the shield, the cutterhead, and the mainbeam. Similarly, the hydraulic circuits of two torque cylinders on the left or right side are connected, leading to the same thrust forces in these cylinders. This treatment enables two pairs of torque cylinders on both sides to generate two independent actuations to adjust the shield's pitch angle and to resist against the tunneling moment about the cutterhead axis. The hydraulic circuits of the left and right oil chambers of the gripper cylinder are connected, leading again to the same thrust forces in these chambers, and thus providing one independent actuation to adjust the shield's yaw angle and to hold two gripper shoes tightly onto the surrounding rock. The above mentioned hydraulic circuit arrangements are clearly depicted by the dashed lines as shown in Fig.2 and Fig.3. Hence, the shield has four controllable movement capabilities in total, i.e. one translation along and one rotation about the cutterhead axis, and two rotations about two axes normal to the cutterhead axis. It is important to note that the shield has two uncontrollable translational movements normal to the cutterhead axis. These movements depend upon the physical boundary conditions exerted by the surrounding rock.

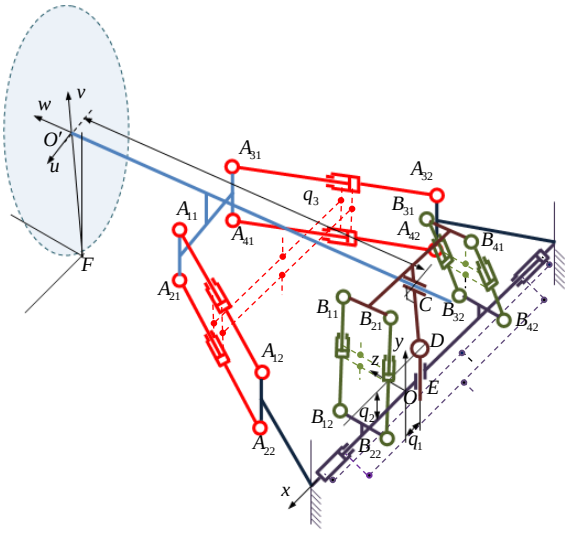

Fig.2. Schematic diagram of the GTRM

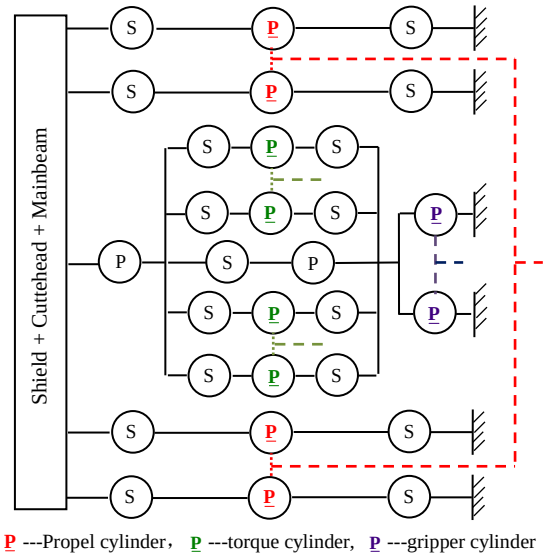

P ---Propel cylinder， P ---torque cylinder, P ---gripper cylinder

Fig.3 Topological structure of the GTRM

3 Inverse Displacement Analysis

In this section, the inverse displacement analysis of the GTRM is carried out for the determination of the lengths and unit vectors of the propel cylinders, torque cylinders and gripper cylinder at a given configuration. In order to achieve that, a reference frame $O-xyz$ is set as shown in Fig.2. Here, the origin O is the center of the central line of the spherical joints situated on the left and right gripper shoe, the x axis is coincident with the gripper cylinder's axis, the y axis is coincident with the vertical axis of the cross pin, and the z axis satisfies the right hand rule. Meanwhile, a body fixed frame $O'-uvw$ attached to the shield is placed. Here, the origin O' is the center of its middle plane, the w axis is coincident with the cutterhead axis, and the u and v axes are parallel to the x and y axes at the initial configuration. In addition, let C be the center of the prismatic joint situated on the saddle with $\left|\overline{CO'}\right| = q_3$, D the center of the cross pin and E the center of the gripper cylinder's axis. Note that the displacements of E relative to O along the x and y axes can be represented by q_1 and q_2 as shown in Fig.2.

Within a thrusting interval, the pose (i.e. position and orientation) of the cutterhead can be described by the position vector $\boldsymbol{r} = \begin{pmatrix} x & y & z \end{pmatrix}^{\mathrm{T}}$ of O', the pitch angle α about the x axis, the yaw angle β about the y axis, and the roll angle γ about the z axis. Since the orientation workspace of the cutterhead is sufficiently small, the rotation matrix of $O'-uvw$ with respect to $O-xyz$ can be approximately expressed as

$$\boldsymbol{R} = \mathrm{Rot}(z,\gamma)\mathrm{Rot}(y,\beta)\mathrm{Rot}(x,\alpha) \approx \begin{bmatrix} 1 & -\gamma & \beta \\ \gamma & 1 & -\alpha \\ -\beta & \alpha & 1 \end{bmatrix} = \begin{bmatrix} \hat{\boldsymbol{u}} & \hat{\boldsymbol{v}} & \hat{\boldsymbol{w}} \end{bmatrix} \tag{1}$$

where $\hat{\boldsymbol{u}}$, $\hat{\boldsymbol{v}}$ and $\hat{\boldsymbol{w}}$ are the unit vectors of three orthogonal axes of the $O'-uvw$.

Thus, at the initial configuration, we have

$$x=0,\ \ y=d,\ \ z=z_0,\ \ \alpha=0,\ \ \beta=0,\ \ \gamma=0$$

where $d=\overline{CD}$ and z_0 denotes the distance from C to O' when the length of each propel cylinder takes the minimum value.

The position vector of O' in the kinematic chain $O-A_{i2}-A_{i1}-O'$ can also be expressed by

$$\boldsymbol{r}=l_{a,i}\boldsymbol{s}_{a,i}+\boldsymbol{a}_{i2}-\boldsymbol{R}\boldsymbol{a}_{0i1},\ \ i=1,\ldots,4 \tag{2}$$

where $\boldsymbol{a}_{0i1}$ and $\boldsymbol{a}_{i2}$ are the position vectors of A_{i1} and A_{i2} evaluated in the $O'-uvw$ and the $O-xyz$ respectively as shown in Fig.4, with

$$\boldsymbol{a}_{011}=\begin{pmatrix}a_{1x} & -a_{1y}+d_a/2 & -a_{1z}\end{pmatrix}^{\mathrm{T}},\ \ \boldsymbol{a}_{021}=\begin{pmatrix}a_{1x} & -a_{1y}-d_a/2 & -a_{1z}\end{pmatrix}^{\mathrm{T}}$$
$$\boldsymbol{a}_{031}=\begin{pmatrix}-a_{1x} & -a_{1y}+d_a/2 & -a_{1z}\end{pmatrix}^{\mathrm{T}},\ \ \boldsymbol{a}_{041}=\begin{pmatrix}-a_{1x} & -a_{1y}-d_a/2 & -a_{1z}\end{pmatrix}^{\mathrm{T}}$$
$$\boldsymbol{a}_{12}=\begin{pmatrix}a_{2x} & d_a/2 & a_{2z}\end{pmatrix}^{\mathrm{T}},\ \ \boldsymbol{a}_{22}=\begin{pmatrix}a_{2x} & -d_a/2 & a_{2z}\end{pmatrix}^{\mathrm{T}}$$
$$\boldsymbol{a}_{32}=\begin{pmatrix}-a_{2x} & d_a/2 & a_{2z}\end{pmatrix}^{\mathrm{T}},\boldsymbol{a}_{42}=\begin{pmatrix}-a_{2x} & -d_a/2 & a_{2z}\end{pmatrix}^{\mathrm{T}}$$

$l_{a,i}$ and $\boldsymbol{s}_{a,i}$ are the length and unit vector of the *i*th propel cylinder.

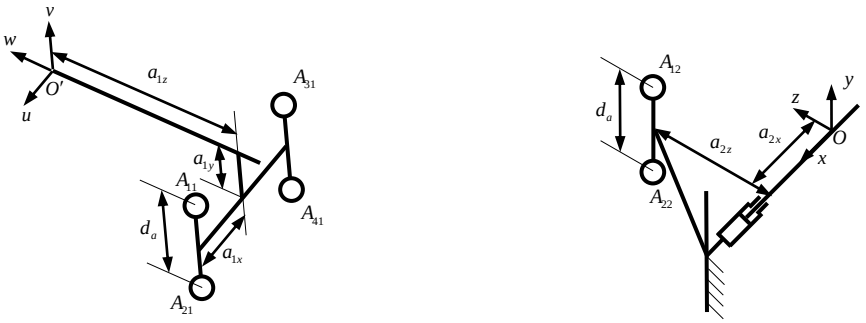

Fig.4 Dimensions of the propel cylinder

At a given configuration of the shield within a tunneling interval, $l_{a,i}$ and $\boldsymbol{s}_{a,i}$ can be determined by

$$l_{a,i}=\sqrt{\left(\boldsymbol{r}-\boldsymbol{a}_{i2}+\boldsymbol{R}\boldsymbol{a}_{0i1}\right)^{\mathrm{T}}\left(\boldsymbol{r}-\boldsymbol{a}_{i2}+\boldsymbol{R}\boldsymbol{a}_{0i1}\right)},\ \ \boldsymbol{s}_{a,i}=\frac{\boldsymbol{r}-\boldsymbol{a}_{i2}+\boldsymbol{R}\boldsymbol{a}_{0i1}}{l_{a,i}} \tag{3}$$

At the initial configuration, we have

$$\boldsymbol{s}_{a,1}=\boldsymbol{s}_{a,2},\ \ \boldsymbol{s}_{a,3}=\boldsymbol{s}_{a,4},\ \ l_{a,1}=l_{a,2}=l_{a,3}=l_{a,4}$$

In addition, the position vector of O' in the kinematic chain $O-D-C-O'$ can be represented by

$$\boldsymbol{r}=-\boldsymbol{R}\boldsymbol{d}_0+\boldsymbol{d} \tag{4}$$

where $\boldsymbol{d}_0=\begin{pmatrix}0 & -d & -q_3\end{pmatrix}^{\mathrm{T}}$ and $\boldsymbol{d}=\begin{pmatrix}q_1 & q_2 & 0\end{pmatrix}^{\mathrm{T}}$ shown in Fig.5 are the position vectors of D evaluated in the $O'-uvw$ and the $O-xyz$, respectively.

Fig.5 Dimensions of the gripper cylinder

Expanding Eq.(4) yields

$$\begin{pmatrix} x \\ y \\ z \end{pmatrix} = \begin{bmatrix} 1 & -\gamma & \beta \\ \gamma & 1 & -\alpha \\ -\beta & \alpha & 1 \end{bmatrix} \begin{pmatrix} 0 \\ d \\ q_3 \end{pmatrix} + \begin{pmatrix} q_1 \\ q_2 \\ 0 \end{pmatrix} = \begin{pmatrix} -\gamma d + \beta q_3 + q_1 \\ d - \alpha q_3 + q_2 \\ \alpha d + q_3 \end{pmatrix} \tag{5}$$

Thus, the displacements of the prismatic joints can be determined by

$$q_1 = x + \gamma d - \beta z\,,\quad q_2 = y - d + \alpha z\,,\quad q_3 = z - \alpha d \tag{6}$$

At the initial configuration, we have

$$q_1 = 0\,,\quad q_2 = 0\,,\quad q_3 = z_0$$

Finally, the position vector of O' in the kinematic chain $O - B_{i2} - B_{i1} - C - O'$ can be represented by

$$\boldsymbol{r} = l_{b,i}\boldsymbol{s}_{b,i} + \boldsymbol{b}_{i2} - \boldsymbol{R}\boldsymbol{b}_{0i1}\,,\quad i = 1,\ldots,4 \tag{7}$$

where $\boldsymbol{b}_{0i1}$ and $\boldsymbol{b}_{i2}$ are the position vectors of B_{i1} and B_{i2} evaluated in the $O' - uvw$ and the $O - xyz$ respectively as shown in Fig.6, with

$$\boldsymbol{b}_{011} = \begin{pmatrix} b_{1x} & b_{1y} & q_3 + d_b/2 \end{pmatrix}^{\mathrm{T}},\ \boldsymbol{b}_{021} = \begin{pmatrix} b_{1x} & b_{1y} & q_3 - d_b/2 \end{pmatrix}^{\mathrm{T}}$$
$$\boldsymbol{b}_{031} = \begin{pmatrix} -b_{1x} & b_{1y} & q_3 + d_b/2 \end{pmatrix}^{\mathrm{T}},\ \boldsymbol{b}_{021} = \begin{pmatrix} -b_{1x} & b_{1y} & q_3 - d_b/2 \end{pmatrix}^{\mathrm{T}}$$
$$\boldsymbol{b}_{12} = \begin{pmatrix} q_1 + b_{2x} & b_{2y} & d_b/2 \end{pmatrix}^{\mathrm{T}}, \boldsymbol{b}_{22} = \begin{pmatrix} q_1 + b_{2x} & b_{2y} & -d_b/2 \end{pmatrix}^{\mathrm{T}}$$
$$\boldsymbol{b}_{32} = \begin{pmatrix} q_1 - b_{2x} & b_{2y} & d_b/2 \end{pmatrix}^{\mathrm{T}}, \boldsymbol{b}_{42} = \begin{pmatrix} q_1 - b_{2x} & b_{2y} & -d_b/2 \end{pmatrix}^{\mathrm{T}}$$

And $l_{b,i}$ and $\boldsymbol{s}_{b,i}$ are the length and unit vector of the *i*th propel cylinder.

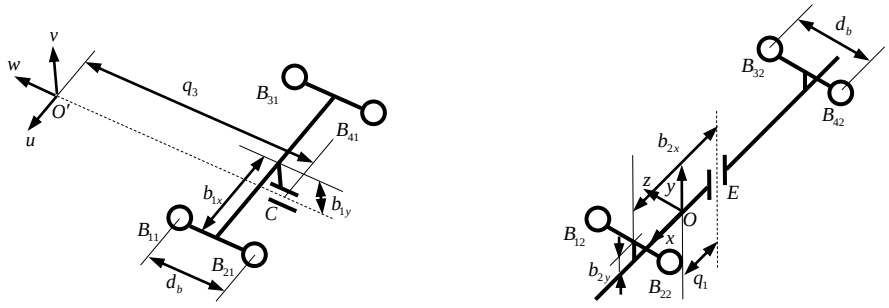

Fig.6 Dimensions of the torque cylinder

Once $\boldsymbol{b}_{0i1}$ and $\boldsymbol{b}_{i2}$ are determined by q_1 and q_3 using Eq.(6), $l_{b,i}$ and $\boldsymbol{s}_{b,i}$ can be obtained by

$$l_{b,i} = \sqrt{\left(\boldsymbol{r} - \boldsymbol{b}_{i2} + \boldsymbol{R}\boldsymbol{b}_{0i1}\right)^{\mathrm{T}}\left(\boldsymbol{r} - \boldsymbol{b}_{i2} + \boldsymbol{R}\boldsymbol{b}_{0i1}\right)}\,,\quad \boldsymbol{s}_{b,i} = \frac{\boldsymbol{r} - \boldsymbol{b}_{i2} + \boldsymbol{R}\boldsymbol{b}_{0i1}}{l_{b,i}}\,,\quad i = 1,\ldots,4 \tag{8}$$

At the initial configuration, we have

$$\boldsymbol{s}_{b,1} = \boldsymbol{s}_{b,2}\,,\quad \boldsymbol{s}_{b,3} = \boldsymbol{s}_{b,4}\,,\quad l_{b,1} = l_{b,2} = l_{b,3} = l_{b,4}$$

4 Static Modeling

This section deals with the inverse and forward force analyses of the GTRM. The gravitational forces of all hydraulic cylinders and the torsional moment between the shield and surrounding rock are assumed to be negligible since they are much smaller than those of other factors.

As shown in Fig.7, the cutterhead-mainbeam-saddle subassembly is taken as the study object in the first place. In Fig.7, the blue arrows are used to indicate the external (tunneling) wrench imposed upon the cutterhead [23], the component gravity, and the drag resistance of ground support equipment, respectively. The red arrows are used to

indicate the thrust forces of the propel cylinders and torque cylinders, the reaction forces at the center of the cross pin, and the friction force between the shield and surrounding rock. Note that the reaction force of the cross pin only contains two components along the *x* and *y* axes since it is a compound joint consisting of a prismatic joint and a spherical joint.

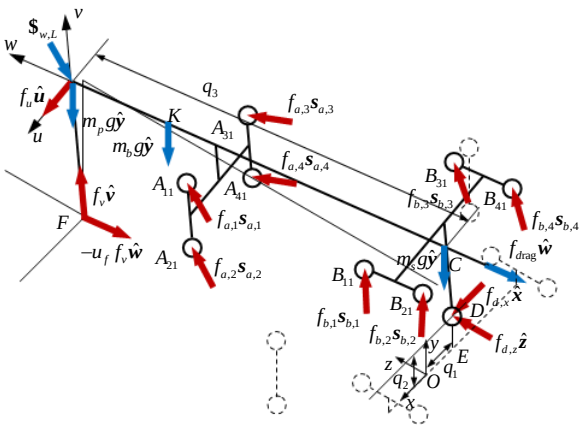

Fig.7 Free-body diagram of the cutterhead-mainbeam-saddle assembly

The symbols shown in Fig.7 are listed as follows:

$\$_{w,L} = \left(\boldsymbol{f}_L^{\mathrm{T}} \quad \boldsymbol{\tau}_L^{\mathrm{T}}\right)^{\mathrm{T}}$ ——the tunneling wrench with respect to O'.

$f_{a,i}$ —the *i*th propel cylinder thrust force.

$f_{b,i}$ —the *i*th torque cylinder thrust force.

$f_{d,x}$, $f_{d,z}$ —the reaction forces of the cross pin at *D* along the *x* and *z* axes.

f_u, f_v —the resultant reaction forces imposed by the surrounding rock to the shield along the *u* and *v* axes at O'.

f_{drag} —the drag resistance of the ground support equipment along the *z* axis.

$\boldsymbol{c}_b$, $\boldsymbol{c}_s$ —the position vectors of the centroids of the main beam and saddle, evaluated in the $O-xyz$.

R —the radius of the shield.

m_p, m_b, m_s ——the masses of the shield (including the cutterhead),the main beam and the saddle.

μ_f —the static friction coefficient of the surrounding rock.

$\boldsymbol{a}_{i1} = \boldsymbol{R}\boldsymbol{a}_{0i1}$, $\boldsymbol{b}_{i1} = \boldsymbol{R}\boldsymbol{b}_{0i1}$ ——the position vectors of A_{i1} and B_{i1} evaluated in the $O-xyz$.

The static force and moment equilibrium equations of the cutterhead-mainbeam-saddle subassembly can be formulated as

$$\boldsymbol{f}_L + f_{\text{drag}}\hat{\boldsymbol{z}} + \left(m_p + m_b + m_s\right)g\hat{\boldsymbol{y}} + \sum_{i=1}^{4} f_{a,i}\boldsymbol{s}_{a,i} + \sum_{i=1}^{4} f_{b,i}\boldsymbol{s}_{b,i} + f_{d,x}\hat{\boldsymbol{x}} + f_{d,z}\hat{\boldsymbol{z}} + f_u\hat{\boldsymbol{u}} + f_v\left(\hat{\boldsymbol{v}} - \mu_f\hat{\boldsymbol{w}}\right) = \boldsymbol{0} \tag{9}$$

$$\boldsymbol{\tau}_L + m_b g\left(\boldsymbol{c}_b \times \hat{\boldsymbol{y}}\right) + m_s g\left(\boldsymbol{c}_s \times \hat{\boldsymbol{y}}\right) + \sum_{i=1}^{4} f_{a,i}\left(\boldsymbol{a}_{i1} \times \boldsymbol{s}_{a,i}\right) + \sum_{i=1}^{4} f_{b,i}\left(\boldsymbol{b}_{i1} \times \boldsymbol{s}_{b,i}\right) + f_{d,x}\left(\boldsymbol{d} \times \hat{\boldsymbol{x}}\right) + f_{d,z}\left(\boldsymbol{d} \times \hat{\boldsymbol{z}}\right) + \mu_f R f_v\hat{\boldsymbol{u}} = \boldsymbol{0} \tag{10}$$

where $\hat{\boldsymbol{x}}$, $\hat{\boldsymbol{y}}$ and $\hat{\boldsymbol{z}}$ denote the unit vectors of three orthogonal axes of the $O-xyz$ frame.

In order to find the relationship between the reaction forces in the cross pin and the thrust forces of the torque and gripper cylinders, the force equilibrium equations of the saddle and the gripper cylinder are formulated using the free body diagrams as shown in Fig.8 and Fig.9.

$$\sum_{i=1}^{4} f_{b,i}\boldsymbol{s}_{b,i} + f_{d,x}\hat{\boldsymbol{x}} + f_{d,z}\hat{\boldsymbol{z}} - m_s g\hat{\boldsymbol{y}} + \boldsymbol{f}_C = \boldsymbol{0} \tag{11}$$

$$-\sum_{i=i}^{4} f_{b,i}\boldsymbol{s}_{b,i} - f_{d,x}\hat{\boldsymbol{x}} - f_{d,z}\hat{\boldsymbol{z}} + \boldsymbol{f}_{h_1} + \boldsymbol{f}_{h2} = \boldsymbol{0} \tag{12}$$

where $\boldsymbol{f}_C$ is the reaction force of the prismatic joint connecting the main beam with the saddle, $\boldsymbol{f}_{h_1}$ and $\boldsymbol{f}_{h2}$ are the reaction forces at the spherical joints of the gripper shoes.

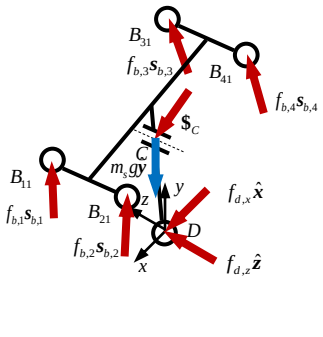

Fig.8 Free-body diagram of the saddle

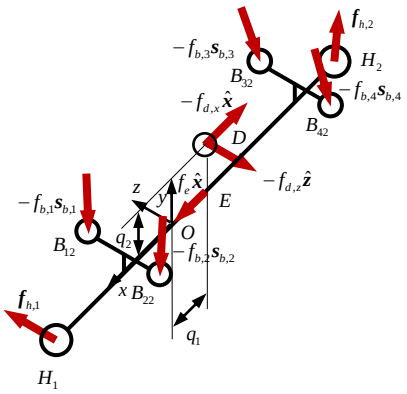

Fig.9 Free-body diagram of the gripper cylinder

Taking the dot product on both sides of Eq.(11) with $\hat{\boldsymbol{w}}$ and that on both sides of Eq.(12) with $\hat{\boldsymbol{x}}$, leads to

$$\sum_{i=1}^{4} f_{b,i}\hat{\boldsymbol{w}}^{\mathrm{T}}\boldsymbol{s}_{b,i} + f_{d,x}\hat{\boldsymbol{w}}^{\mathrm{T}}\hat{\boldsymbol{x}} + f_{d,z}\hat{\boldsymbol{w}}^{\mathrm{T}}\hat{\boldsymbol{z}} - m_s g\hat{\boldsymbol{w}}^{\mathrm{T}}\hat{\boldsymbol{y}} = 0 \tag{13}$$

$$f_{d,x} = f_e - \sum_{i=1}^{4} f_{b,i}\hat{\boldsymbol{x}}^{\mathrm{T}}\boldsymbol{s}_{b,i} \quad f_{d,x} = f_e - \sum_{i=1}^{4} f_{b,i}\hat{\boldsymbol{x}}^{\mathrm{T}}\boldsymbol{s}_{b,i} \tag{14}$$

where $f_e = \left(\boldsymbol{f}_{h_1} + \boldsymbol{f}_{h_2}\right)^{\mathrm{T}}\hat{\boldsymbol{x}}$ denotes the trust force in the gripper cylinder.

Substituting Eq.(14) into Eq.(13), results in

$$f_{d,z} = -\frac{1}{\hat{\boldsymbol{w}}^{\mathrm{T}}\hat{\boldsymbol{z}}}\left(\sum_{i=1}^{4} f_{b,i}\hat{\boldsymbol{w}}^{\mathrm{T}}\boldsymbol{s}_{b,i} + \left(f_e - \sum_{i=i}^{4} f_{b,i}\hat{\boldsymbol{x}}^{\mathrm{T}}\boldsymbol{s}_{b,i}\right)\hat{\boldsymbol{w}}^{\mathrm{T}}\hat{\boldsymbol{x}} - m_s g\hat{\boldsymbol{w}}^{\mathrm{T}}\hat{\boldsymbol{y}}\right) \tag{15}$$

This means that the reaction forces of the cross pin $f_{d,x}$ and $f_{d,z}$ can be expressed as a function of the thrust forces of the gripper and torque cylinders, as well as the saddle's gravity.

Substituting Eqs.(14) and (15) into Eqs.(9) and (10) results in

$$\$_w = \sum_{i=1}^{4} f_{a,i}\$_{w,a,i} + \sum_{i=1}^{4} f_{b,i}\$_{w,b,i} + f_e\$_{w,e} + f_u\$_{w,u} + f_v\$_{w,v} \tag{16}$$

where

$$\$_w = \begin{pmatrix} \boldsymbol{f}_L + \left(m_p + m_s + m_b\right)g\hat{\boldsymbol{y}} + f_{\mathrm{drag}}\hat{\boldsymbol{z}} - \dfrac{m_s g\hat{\boldsymbol{w}}^{\mathrm{T}}\hat{\boldsymbol{y}}}{\hat{\boldsymbol{z}}^{\mathrm{T}}\hat{\boldsymbol{w}}}\hat{\boldsymbol{z}} \\ \boldsymbol{\tau}_L + \left(m_b g\boldsymbol{c}_b + m_s g\boldsymbol{c}_s\right)\times\hat{\boldsymbol{y}} - \dfrac{m_s g\hat{\boldsymbol{w}}^{\mathrm{T}}\hat{\boldsymbol{y}}}{\hat{\boldsymbol{z}}^{\mathrm{T}}\hat{\boldsymbol{w}}}\left(\boldsymbol{d}\times\hat{\boldsymbol{z}}\right) \end{pmatrix}$$

$$\$_{w,a,i} = \begin{pmatrix} \boldsymbol{s}_{a,i} \\ \boldsymbol{a}_{i1}\times\boldsymbol{s}_{a,i} \end{pmatrix}, \quad \$_{w,b,i} = \begin{pmatrix} \boldsymbol{s}_{b,i} - \dfrac{1}{\hat{\boldsymbol{z}}^{\mathrm{T}}\hat{\boldsymbol{w}}}\left(\hat{\boldsymbol{x}}^{\mathrm{T}}\boldsymbol{s}_{b,i}\hat{\boldsymbol{n}} + \hat{\boldsymbol{w}}^{\mathrm{T}}\boldsymbol{s}_{b,i}\hat{\boldsymbol{z}}\right) \\ \boldsymbol{b}_{i1}\times\boldsymbol{s}_{b,i} - \dfrac{1}{\hat{\boldsymbol{z}}^{\mathrm{T}}\hat{\boldsymbol{w}}}\boldsymbol{d}\times\left(\hat{\boldsymbol{x}}^{\mathrm{T}}\boldsymbol{s}_{b,i}\hat{\boldsymbol{n}} + \hat{\boldsymbol{w}}^{\mathrm{T}}\boldsymbol{s}_{b,i}\hat{\boldsymbol{z}}\right) \end{pmatrix}$$

$$\$_{w,e} = \frac{1}{\hat{\boldsymbol{z}}^{\mathrm{T}}\hat{\boldsymbol{w}}}\begin{pmatrix} \hat{\boldsymbol{n}} \\ \boldsymbol{d}\times\hat{\boldsymbol{n}} \end{pmatrix}, \quad \$_{w,u} = \begin{pmatrix} \hat{\boldsymbol{u}} \\ \boldsymbol{0} \end{pmatrix}, \quad \$_{w,v} = \begin{pmatrix} \hat{\boldsymbol{v}} - \mu_f\hat{\boldsymbol{w}} \\ -R\mu_f\hat{\boldsymbol{u}} \end{pmatrix}, \quad \hat{\boldsymbol{n}} = \hat{\boldsymbol{y}}\times\hat{\boldsymbol{w}}$$

It is worthwhile pointing out again that unlike the redundantly actuated parallel mechanisms where all actuators are assumed to be linearly independent [22], the hydraulic systems in the GTRM are elaborately designed in the following ways to avoid presence of pre-stress possibly arising from redundant actuation. The hydraulic circuits of all four propel cylinders are connected and their piston's cross sections are identical. Consequently, the thrust forces of these cylinders are the same in magnitude, i.e.

$$f_{a,i} = f_{a,2} = f_{a,3} = f_{a,4} = f_a \tag{17}$$

Meanwhile, the hydraulic circuits of two torque cylinders on each side are connected and their piston's cross sections

are identical, leading to the same thrust forces in these cylinders, i.e.

$$f_{b,1} = f_{b,2} = f_{bl}\ , \quad f_{b,3} = f_{b,4} = f_{br} \tag{18}$$

Hence, substituting Eqs.(17)-(18) into Eq.(16) , finally results in the force model of the GTRM.

$$\$_w = \boldsymbol{W}\boldsymbol{\rho}_w \tag{19}$$

$$\boldsymbol{W} = \begin{bmatrix} \boldsymbol{W}_a & \boldsymbol{W}_c \end{bmatrix},\ \boldsymbol{W}_a = \begin{bmatrix} \lambda_a \hat{\$}_{w,a} & \lambda_{bl} \hat{\$}_{w,bl} & \lambda_{br} \hat{\$}_{w,br} & \lambda_e \hat{\$}_{w,e} \end{bmatrix},\ \boldsymbol{W}_c = \begin{bmatrix} \lambda_u \hat{\$}_{w,u} & \lambda_v \hat{\$}_{w,v} \end{bmatrix}$$

$$\lambda_a \hat{\$}_{w,a} = \frac{1}{4}\sum_{i=1}^{4} \$_{w,a,i} \quad \lambda_{bl} \hat{\$}_{w,bl} = \frac{1}{2}\sum_{i=1}^{2} \$_{w,b,i} \quad \lambda_{br} \hat{\$}_{w,br} = \frac{1}{2}\sum_{i=3}^{4} \$_{w,b,i}\ , \quad \$_{w,e} = \lambda_e \hat{\$}_{w,e} \quad \hat{\$}_{w,u} = \$_{w,u} \quad \lambda_v \hat{\$}_{w,v} = \$_{w,v}$$

$$\boldsymbol{\rho}_w = \begin{pmatrix} \boldsymbol{\rho}_{wa}^{\mathrm{T}} & \boldsymbol{\rho}_{wc}^{\mathrm{T}} \end{pmatrix}^{\mathrm{T}},\ \boldsymbol{\rho}_{wa} = \begin{pmatrix} 4f_a & 2f_{bl} & 2f_{br} & f_e \end{pmatrix}^{\mathrm{T}},\ \boldsymbol{\rho}_{wc} = \begin{pmatrix} f_u & f_v \end{pmatrix}^{\mathrm{T}}$$

where $\$_w$ is the equivalent externally applied wrench imposed upon the shield, which is composed of the wrenches due to the tunneling loads, gravity and drag resistance of the ground support equipment. $\hat{\$}_{w,a}$, $\hat{\$}_{w,bl}$, $\hat{\$}_{w,br}$ and $\hat{\$}_{w,e}$ denote the equivalent unit wrench of actuations imposed upon the shield by the propel cylinders, the left and right torque cylinders, and the gripper cylinder. $\hat{\$}_{w,u}$ and $\hat{\$}_{w,v}$ denote the equivalent unit wrench of constraints imposed upon the shield by surrounding rock. $\boldsymbol{W}$ is a 6×6 matrix known as the force Jacobian that maps the equivalent actuated and virtual joint forces onto the externally applied wrench. $\boldsymbol{W}_a$ and $\boldsymbol{W}_c$ are known respectively as the force Jacobian of actuations and constraints.

In order to facilitate the forward and inverse force analyses, the equivalent externally applied wrench is decomposed into two components

$$\$_w = \$_{w,L} + \$_{w,G} \tag{20}$$

where $\$_{w,G}$ represents the wrench caused by gravity and drag resistance. It is important to note that the tunneling wench $\$_{w,L}$ is always evaluated in the $O'-uvw$ and its components along the v and u axes are negligible[24]. Partitioning $\$_{w,L}$ and $\$_{w,G}$ according to the controllable and uncontrollable degrees of freedom, leads to

$$\$_{w,L} = \boldsymbol{T}\$'_{w,L} = \boldsymbol{T}\begin{pmatrix} 0 \\ 0 \\ f'_{L,w} \\ \tau'_{L,u} \\ \tau'_{L,v} \\ \tau'_{L,w} \end{pmatrix} = \boldsymbol{T}\begin{pmatrix} \boldsymbol{0}_{2\times 1} \\ \boldsymbol{f}'_{La} \end{pmatrix},\ \$_{w,G} = \begin{pmatrix} \left(m_p + m_s + m_b\right) g\hat{\boldsymbol{y}} + f_{\mathrm{drag}}\hat{\boldsymbol{z}} - \dfrac{m_s g \hat{\boldsymbol{w}}^{\mathrm{T}}\hat{\boldsymbol{y}}}{\hat{\boldsymbol{z}}^{\mathrm{T}}\hat{\boldsymbol{w}}}\hat{\boldsymbol{z}} \\ \left(m_b g\boldsymbol{c}_b + m_s g\boldsymbol{c}_s\right)\times\hat{\boldsymbol{y}} - \dfrac{m_s g\hat{\boldsymbol{w}}^{\mathrm{T}}\hat{\boldsymbol{y}}}{\hat{\boldsymbol{z}}^{\mathrm{T}}\hat{\boldsymbol{w}}}\left(\boldsymbol{d}\times\hat{\boldsymbol{z}}\right) \end{pmatrix} = \begin{pmatrix} \boldsymbol{f}_{Gc} \\ \boldsymbol{f}_{Ga} \end{pmatrix},\ \boldsymbol{T} = \begin{bmatrix} \boldsymbol{R} & \\ & \boldsymbol{R} \end{bmatrix} \tag{21}$$

Consequently, Eq. (20) can be rewritten as

$$\begin{pmatrix} \boldsymbol{0}_{2\times 1} \\ \boldsymbol{f}'_{La} \end{pmatrix} = \boldsymbol{T}^{\mathrm{T}}\begin{bmatrix} \boldsymbol{W}_{ca} & \boldsymbol{W}_{cc} \\ \boldsymbol{W}_{aa} & \boldsymbol{W}_{ac} \end{bmatrix}\begin{pmatrix} \boldsymbol{\rho}_{wa} \\ \boldsymbol{\rho}_{wc} \end{pmatrix} - \boldsymbol{T}^{\mathrm{T}}\begin{pmatrix} \boldsymbol{f}_{Gc} \\ \boldsymbol{f}_{Ga} \end{pmatrix} = \begin{bmatrix} \boldsymbol{W}'_{ca} & \boldsymbol{W}'_{cc} \\ \boldsymbol{W}'_{aa} & \boldsymbol{W}'_{ac} \end{bmatrix}\begin{pmatrix} \boldsymbol{\rho}_{wa} \\ \boldsymbol{\rho}_{wc} \end{pmatrix} - \begin{pmatrix} \boldsymbol{f}'_{Gc} \\ \boldsymbol{f}'_{Ga} \end{pmatrix} \tag{22}$$

On one hand, suppose that $\boldsymbol{f}'_{La} = \begin{pmatrix} f'_{L,w} & \tau'_{L,u} & \tau'_{L,v} & \tau'_{L,w} \end{pmatrix}^{\mathrm{T}}$ can be estimated using the geological conditions and tunneling parameters, the required $\boldsymbol{\rho}_{wa}$ and $\boldsymbol{\rho}_{wc}$ can then be obtained by

$$\boldsymbol{\rho}_{wc} = -\boldsymbol{W}'^{-1}_{cc}\left(\boldsymbol{W}'_{ca}\boldsymbol{\rho}_{wa} - \boldsymbol{f}'_{Gc}\right),\ \boldsymbol{\rho}_{wa} = \left(\boldsymbol{W}'_{aa} - \boldsymbol{W}'_{ac}\boldsymbol{W}'^{-1}_{cc}\boldsymbol{W}'_{ca}\right)^{-1}\left(\boldsymbol{f}'_{La} + \boldsymbol{f}'_{Ga} - \boldsymbol{W}'_{ac}\boldsymbol{W}'^{-1}_{cc}\boldsymbol{f}'_{Gc}\right) \tag{23}$$

On the other hand, suppose that the thrust forces of hydraulic cylinders can be obtained by pressure sensors and low-pass filters, $\boldsymbol{f}'_{La}$ can in turn be estimated by

$$\boldsymbol{f}'_{La} = \left(\boldsymbol{W}'_{aa} - \boldsymbol{W}'_{ac}\boldsymbol{W}'^{-1}_{cc}\boldsymbol{W}'_{ca}\right)\boldsymbol{\rho}_{wa} + \boldsymbol{W}'_{ac}\boldsymbol{W}'^{-1}_{cc}\boldsymbol{f}'_{Gc} - \boldsymbol{f}'_{Ga} \tag{24}$$

Eqs.(23) and (24) embody the merits of this article.

5 Example

By taking a GTRM whose cutterhead diameter is eight meters as an example, we demonstrate how to use the force model developed in Section 3 to estimate the thrust forces of hydraulic cylinders using the estimated tunneling loads in the design stage, and to predict the tunneling loads using the measured thrust forces in an actual tunneling process. The geometric and physical parameters given in [25] for the simulation are listed in Table 1 and Table 2.

Table 1 Geometrical parameters

Parameter	Value(mm)	Parameter	Value(mm)
a_{1x}	1648	d_b	6248
a_{1y}	286	b_{2x}	656
a_{1z}	6248	b_{2y}	1914
d_a	1143	d	7800
a_{2x}	3185	q_1	0
a_{2z}	1836	q_2	0
b_{1x}	1258	q_3	11964
b_{1y}	1900		

Table 2 Workspace and physical parameters

Parameter	Value
Thrusting stroke	$L=1800$ mm
Orientation capabilities	$-0.718 \le \alpha \le 0.718^\circ$, γ=0 $-1.676 \le \beta \le 1.676^\circ$
Friction coefficient	0.3
Drag resistance	$f_{drag}=2100$ KN
Component gravity	Cutterhead $m_p g=4500$ KN Main beam $m_b g=1200$ KN Saddle $m_s g=300$ KN

(1) Inverse force analysis: The rated tunneling force F along and the rated tunneling moment M about the cutterhead axis (the w axis) are approximately estimated using the empirical formulas given in [26]

$$F=n\sigma,\ M=SD^2$$

where n is the number of cutters, σ is the cutter rated load, D is the cutterhead's diameter, and S is the torque coefficient. By taking $n=60$, $\sigma=300$, S=60, $D=8$, and considering adequate unbalanced moments about the u and v axes according to [27], we have

$$\boldsymbol{f}'_{La}=\left(18000\text{KN}\quad 1000\text{KNm}\quad 100\text{KNm}\quad 3840\text{KNm}\right)^{\mathrm{T}}$$

Fig.10 shows the variations of the thrust forces of the propel cylinder, the left (right) torque cylinder and the gripper cylinder versus l, ($l=z-z_0$), α and β provided that $\boldsymbol{f}'_{La}$ keeps unchanged within a thrusting interval. Therefore, the absolute maximum thrust forces of the cylinders required to resist against the tunneling loads can be determined, a key step in the design of the hydraulic systems.

(2) Forward force analysis: Suppose that the thrust forces of all hydraulic cylinders have been detected by the pressure sensors at the initial configuration ($l=0,\ \alpha=0,\ \beta=0$) such that

$$f_a=5489\text{ KN},\quad f_{b,l}=838\text{ KN},\quad f_{b,r}=259\text{ KN},\quad f_e=0\text{ KN}$$

The tunneling loads can then be estimated by Eq.(24)

$$\boldsymbol{f}'_{La}=\left(15700\text{KN}\quad 10\text{KNm}\quad 0\text{KNm}\quad 2540\text{KNm}\right)^{\mathrm{T}}$$

It is easy to see that the unbalanced moments in this case are negligible. Now, suppose that three cases of thrust forces of the hydraulic cylinder maybe detected at the end of the tunneling interval where the orientation of the cutterhead keeps unchanged （$l=1800,\ \alpha=0,\ \beta=0$）. Then, the tunneling loads given in Table 3 can be predicted using Eq.(23) for each case.

It is also observed that the tunneling force/moment along/about the cutterhead axis increases compared with that at the initial configuration and the unbalanced moments about the u and v axes are negligible for Case 1. The tunneling force/moment along/about the cutterhead axis keeps almost unchanged compared with that at the initial configuration and the unbalanced moment about the x axis occurs for Case 2. The tunneling force/moment along/about the cutterhead axis decreases compared with that at the initial configuration and the unbalanced moment about the y axis occurs for Case 3. For the last two cases, appropriate rectifications should be made accordingly. The other cases encountered in practice can also be treated in the similar manner.

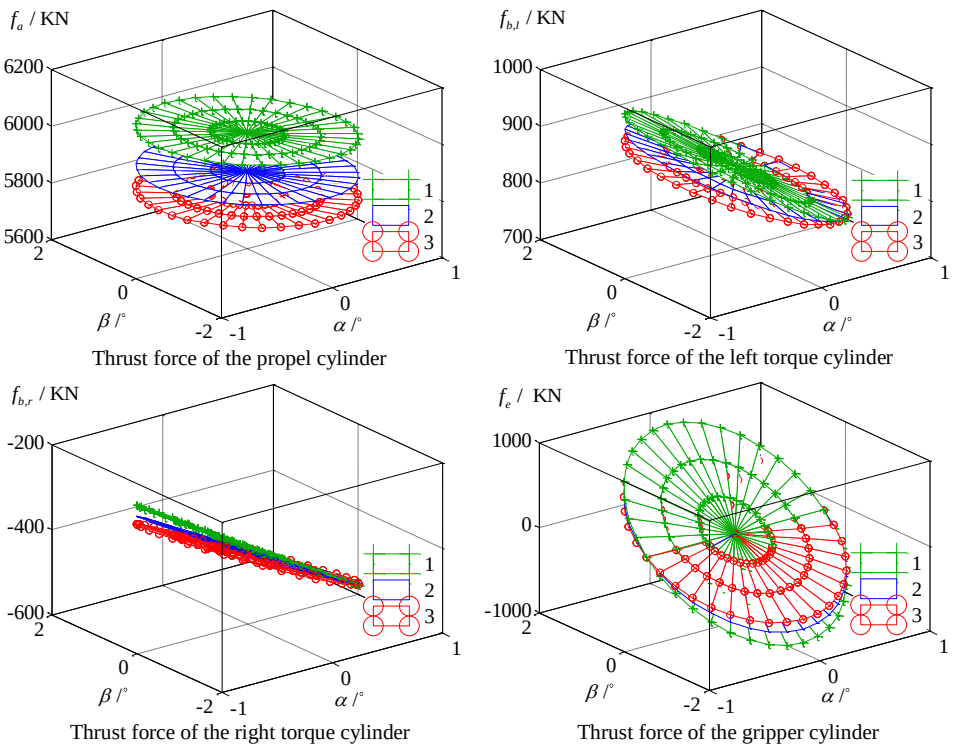

1-l=0 mm, 2-l=900 mm, 3-l=1800 mm

Fig.10 Variations of the thrust forces versus l, α and β

Table 3 Estimations of the tunneling loads using the thrust forces

Number	f_a	$f_{b,l}$	$f_{b,r}$	f_e	$\boldsymbol{f}'_{La}$
1	5840	912	229	0	[17000;48;0;3000]
2	5329	742	171	0	[15026;3033;0;2506]
3	5039	787	247	86	[14035;70;1029;2398]

6 Conclusions

This paper presents an approach for force analysis of an open TBM GTRM and the following conclusions are drawn:

(1) The GTRM is a special parallel mechanism driven by multiple hydraulic cylinders and working under constraints of surrounding rock. Since the hydraulic circuits of four propel cylinders are connected, and so are those of the torque cylinders and the gripper cylinder on the left and right side, the mechanism has four independent actuations.

(2) The models for the forward and inverse force analyses of the GTRM have been developed. These models can be used to estimate the thrust forces of the hydraulic cylinders required to resist the tunneling loads, and to predict the tunneling loads provided that the trust forces in the cylinders can be obtained by measurements. They thereby provide important theoretical basis for the design and control of the mechanism.

Acknowledgements

This research work was partially supported by the National Key Basic Research Program under grant 2013CB035403 and the National High Technology Research and Development Program under grant 2012AA041803.

References

[1] M Ramoni, G Anagnostou, Tunnel boring machines under squeezing conditions, Tunnelling and Underground Space Technology, 2010, 25:139-157.

[2] E Farrokh, J Rostami, C Laughton, Analysis of unit supporting time and support installation time for open TBMs, Rock Mechanics and Rock Engineering, 2011, 44(4):431-445.

[3] B Dasgupta, T S Mruthyunjaya, A Newton-Euler formulation for the inverse dynamics of the Stewart platform manipulator, Mechanism and Machine Theory, 1998, 33(8):1135-1152.

[4] B Dasgupta, T S Mruthyunjaya, Closed-form dynamic equations of the general Stewart platform through the Newton–Euler approach, Mechanism and Machine Theory, 1998, 33(97):993-1012.

[5] M S Tsai, W H Yuan, Inverse dynamics analysis for a 3-PRS parallel mechanism based on a special decomposition of the

reaction forces, Mechanism and Machine Theory, 2010, 45:1491-1508.
[6] T N Shiau, Y J Tsai, M S Tsai, Nonlinear dynamic analysis of a parallel mechanism with consideration of joint effects, Mechanism and Machine Theory, 2008, 43(4):491-505.
[7] S Briot, V Glazunov, V Arakelian, Investigation on the effort transmission in planar parallel manipulators, Journal of Mechanisms and Robotics, 2013, 5(1):46-59.
[8] K J Waldron, K H Hunt, Series-parallel dualities in actively coordinated mechanisms, International Journal of Robotics Research, 1988, 10(5):473-480.
[9] C Gosselin, Stiffness mapping for parallel manipulator, Robotics and Automation IEEE Transactions on, 1990, 6(3):377-382.
[10] S Joshi, L W Tsai, A comparison study of two 3-DOF parallel manipulators: one with three and the other with four supporting legs, Robotics and Automation IEEE Transactions on, 2003, 19(2):3690-3697.
[11] L W Tasi, S Joshi, Kinematic analysis of 3-DOF position mechanisms for use in hybrid kinematic machines, Journal of Mechanical Design, 2002, 124(2):245-253.
[12] F Pierrot, O Company, Modeling and design issues of a 3-axis parallel machine-tool, Mechanism and Machine Theory, 2002, 37(11):1325-1345.
[13] F Majou, C Gosselin, P Wenger, et al, Parametric stiffness analysis of the Orthoglide, Mechanism and Machine Theory, 2007, 42(3):296-311.
[14] S A Joshi, L W Tsai, Jacobian analysis of limited-DOF parallel manipulators, Journal of Mechanical Design, 2002, 124(2):341-348.
[15] Y D Xu, W L Liu, J T Yao, et al, A method for force analysis of the overconstrained lower mobility parallel mechanism, Mechanism and Machine Theory, 2015, 88:31-48.
[16] Q S Xu, Y M Li, An investigation on mobility and stiffness of a 3-DOF translational parallel manipulator via screw theory, Robotics and Computer-Integrated Manufacturing, 2008, 24(3):402-414.
[17] T Huang, H T Liu, D G Chetwynd, Generalized Jacobian analysis of lower mobility manipulators, Mechanism and Machine Theory, 2011, 46(6):831-844.
[18] M Zoppi, D Zlatanov, R M Molfino, On the velocity analysis of interconnected chains mechanisms, Mechanism and Machine Theory, 2006, 41(11):1346-1358.
[19] C A Yazdani, S H Yakhchali, Tunnel Boring Machine (TBM) selection using fuzzy multicriteria decision making methods, Tunnelling and Underground Space Technology, 2012, 30(4):194-204.
[20] R Hasanpour, J Rostami, B Unver, 3D finite difference model for simulation of double shield TBM tunneling in squeezing grounds, Tunneling and Underground Space Technology, 2014, 40(2):109-126.
[21] M Ramoni, G Anagnostou. Tunnel boring machines under squeezing conditions, Tunneling and Underground Space Technology, 2010, 25:139-157.
[22] A Müller, On the terminology and geometric aspects of redundant parallel manipulators, Robotica, 2013, 31(1):137-147.
[23] J Rostami, Development of a force estimation model for rock fragmentation with disc cutters through theoretical modeling and physical measurement of crushed zone pressure, Colorado: Colorado School of Mines, 1997.
[24] J Rostami, L Ozdemir. Computer modeling of mechanical excavators cutterhead//Proceedings of the World Rock Boring Association Conference, Ontario (1996).
[25] Service manual tunnel boring machine model MB264-311, America: The Robbins Company, 2009.
[26] Y L Du, L J Du, et al, Full face hard rock tunnel boring machine—system principles and integrated design, Wuhan: Huazhong University of Science and Technology Press, 2011. (in Chinese).
[27] X X Zeng, H D Yu, K Z Zhang, et al, Bending moments study on the cutterheads of shield machines excavating in composition geologic strata, Journal of Shanghai Jiaotong University, 2010. (in Chinese).

Listing of figure captions:

Table 1. Geometrical parameters

Parameter	Value(mm)	Parameter	Value(mm)
a_{1x}	1648	d_b	6248
a_{1y}	286	b_{2x}	656
a_{1z}	6248	b_{2y}	1914
d_a	1143	d	7800
a_{2x}	3185	q_1	0
a_{2z}	1836	q_2	0
b_{1x}	1258	q_3	11964
b_{1y}	1900		

Table 2. Workspace and physical parameters

Parameter	Value
Thrusting stroke	$L = 1800$ mm
Orientation capabilities	$-0.718 \le \alpha \le 0.718^{\circ}$, γ=0 $-1.676 \le \beta \le 1.676^{\circ}$
Friction coefficient	0.3
Drag resistance	$f_{drag} = 2100$ KN
Component gravity	Cutterhead $m_p g = 4500$ KN Main beam $m_b g = 1200$ KN Saddle $m_s g = 300$ KN

Table 3 Estimations of the tunneling loads using the thrust forces

Number	f_a	$f_{b,l}$	$f_{b,r}$	f_e	$\boldsymbol{F}_a'$
1	5840	912	229	0	[17000;48;0;3000]
2	5329	742	171	0	[15026;3033;0;2506]
3	5039	787	247	86	[14035;70;1029;2398]